NOTES AND CORRESPONDENCE
A Case Study of a Quasistationary,
Very Long Polar Stratospheric Cloud Layer Edge

Peter VOELGER and Peter DALIN

Swedish Institute of Space Physics, Sweden

Abstract

A case study of the occurrence of polar stratospheric clouds (PSCs) on February 13th, 2017, in northern Sweden is reported in this paper. For the first time, a quasistationary edge of a bright and extended PSC layer (~ 600-km long) on the eastern side of the Scandinavian mountain range was photographed and registered using lidar observations. Both lidar measurements and model simulations demonstrated that atmospheric conditions were fairly unchanged for several hours during the presence of the PSC. Strong winds across the Scandinavian mountain range were responsible for triggering the formation of mountain lee waves in the Kiruna area, which induced the formation of the quasistationary long and straight edge of the PSCs.

1. Introduction

Polar stratospheric clouds (PSCs) are a common phenomenon during Arctic and Antarctic wintertime. Their formation requires the stratospheric temperature to fall below ~ 195 K (e.g., Browell et al. 1990; Taba-zadeh et al. 1994; Larsen et al. 1997). The formation temperature is typically only reached inside the polar vortex. Temperatures over the Arctic tend to be higher than those over Antarctica since the Arctic vortex is more unstable. Therefore, PSCs occur more frequently over Antarctica (Maturilli et al. 2005; Tilmes et al. 2006; Spang et al. 2016). This also means that PSC formation in the Arctic is more strongly influenced by atmospheric disturbances such as waves (Carslaw

et al. 1998; Kohma and Sato 2011; Alexander et al. 2013). Sources for waves can be wind shear in the troposphere (e.g., the polar jet stream) or topographic features such as ridges and mountain chains. One well-known and well-documented source in Northern Europe is the Scandinavian mountain range (see, e.g., Dörnbrack and Leutbecher 2001; Blum et al. 2004; Kirkwood et al. 2010; Kaifler et al. 2017). Waves originating at the mountain range are known to produce temperature modulations due to vertical motion of air that allow the formation of PSCs at certain locations downstream (Voigt et al. 2000; Dörnbrack et al. 2002).

In an ideal case, the uniform flow across a straight mountain ridge should result in a wave-like modulation of temperature downstream, with no variations parallel to the ridge. This would lead to long crests of clouds (see, e.g., Fig. 16 of Fritts and Alexander 2003). In reality, clouds in the lee of the Scandinavian mountain range have more complex, patchy structures. Reasons are inhomogeneities in the horizontal wind field (hor-

Fig. 1.   Photographs of PSC in the WSW direction (left) and the ENE direction (right), taken on February 13th, 2017 at 14:31 UT and 16:08 UT, respectively, in Kiruna (Sweden).

izontal wind shears), either due to local topographic effects or mesoscale variations. PSCs over Kiruna have been documented photographically for many years (see https://doi.org/10.34474/data.jmsj.13488744 and http://data.irf.se/data/dalin2020psc). Based on those observations, it can be concluded that clouds with patchy structures are common over Kiruna, while well-defined cloud boundaries are a rare exception.

In the present paper, we discuss an unusual case in which a PSC layer, which formed due to mountain lee waves, had an extended edge and remained stationary over a rather long period of time. In the following section, we first explain the instruments and methods that were used in this study. Thereafter, the observations are described, followed by their interpretation and a summary.

2.   Instruments and methods

This study is based on a combination of optical observations and model data. Photographic images were taken with a Canon G5 camera (resolution of 2,592 × 1,944 pixels) from the roof of the main building of the Swedish Institute of Space Physics in Kiruna, Northern Sweden (IRF, located at 67.84°N, 20.41°E). Lidar measurements were performed with a backscatter lidar located at IRF. The lidar operates at a wavelength of 532 nm and has two detection channels that distinguish parallel and perpendicular polarization of the backscattered light. The altitude range for observations is 5−50 km. Height and time resolutions are 30 m and 133 s, respectively (see Voelger and Nikulin (2005) for more details).

For interpretation of atmospheric conditions during the period of interest, simulations were performed

using the Weather Research and Forecasting (WRF) model (Skamarock et al. 2008). WRF allows the calculation of the state of the atmosphere on a user-defined 3D grid for chosen time steps. As input for WRF, we used ERA5 reanalysis data from the European Centre for Medium-Range Weather Forecasts. ERA5 data have a horizontal resolution of 31 km and 137 vertical levels (Hersbach et al. 2020).

3.   Observational data

Images of a polar stratospheric cloud were taken in Kiruna (67.84°N, 20.41°E) in the afternoon of February 13th, 2017 (Fig. 1). The cloud edge was unusual in that it (a) remained at the same location for several hours (at least during the period of visual and photographic observations 14−17 UT, corresponding to 15−18 LT) and (b) was long and straight (modulated with filaments) along a line from southwest to northeast as long as approximately 600 km at least. Based on geographical features on the photographic images (e.g., mountains and the position of the sunset), it was possible to determine the angle between geographical north and the cloud edge to be 44° ± 5° (Fig. 2). Concurrently, winds were consistently blowing from directions between north and northwest, hence approximately along the normal of the cloud edge. Wind speed at the ground was between 6 and 8 m s^{-1} as recorded by IRF's weather station. Such wind conditions are favorable for the formation of mountain gravity waves on the lee side of the Scandinavian mountain range, i.e. on its eastern side. This strengthens the assumption that the cloud frontal shape is a result of mountain gravity waves.
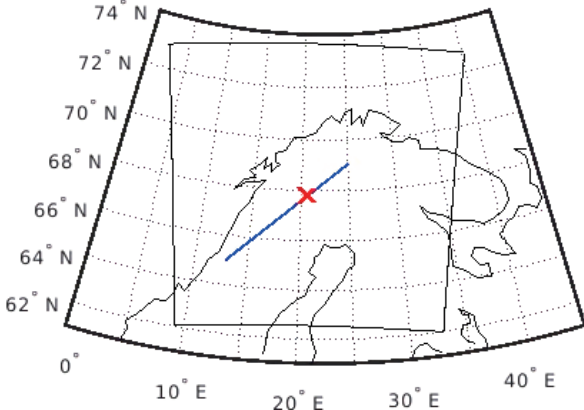
During the following night, IRF's backscatter

Fig. 2.   Estimated front of the observed PSC based on sunset and on identification of topographic features that are visible in the photographs in Fig. 1. Thin black lines mark the edges of the grid used in WRF simulations.

3). In lidar measurements, PSCs can be characterized by (a) the depolarization ratio $\delta = I_{perp}/I_{par}$, with I_{par} and I_{perp} being the measured backscatter intensity of the parallel and perpendicular channels, respectively, and (b) the backscatter ratio R, defined as $R = (\beta_{psc} + \beta_{mol})/\beta_{mol}$, where β_{psc} and β_{mol} is the backscatter coefficient for PSCs and molecules, respectively. The combination of R and δ allows for the determination of the chemical composition of the cloud (see Browell et al. 1990 for details). In the case discussed here, the combination of the large backscatter ratio and the large depolarization ratio indicated that the cloud consisted of ice particles. Over Northern Scandinavia, such clouds are mostly only formed in connection with mountain gravity waves (Blum et al. 2005).

4.   Data analysis

To put our local observations in a regional context, we examined atmospheric conditions with the help of WRF simulations. The model grid covered the northern part of Fennoscandia with 5.4 km distance between horizontal grid points and 160 height levels up to 10 hPa (see Fig. 2 for area covered by grid). Simulations were performed for a period of 96 hours, starting at 48 hours before the photos were taken. Time resolution of the output was set to 10 min.

Figure 4 indicates simulated wind and temperature fields at a 25 km altitude for 12 and 18 UT on date

lidar was performing measurements 1 km south of the location where the photos were taken. The lidar operated from 17 UT until next morning 04:45 UT. Backscatter signals with both parallel and perpendicular polarization were recorded. During the whole observation period, a cloud layer was present in the stratosphere between 24 km and 27 km altitude (Fig.
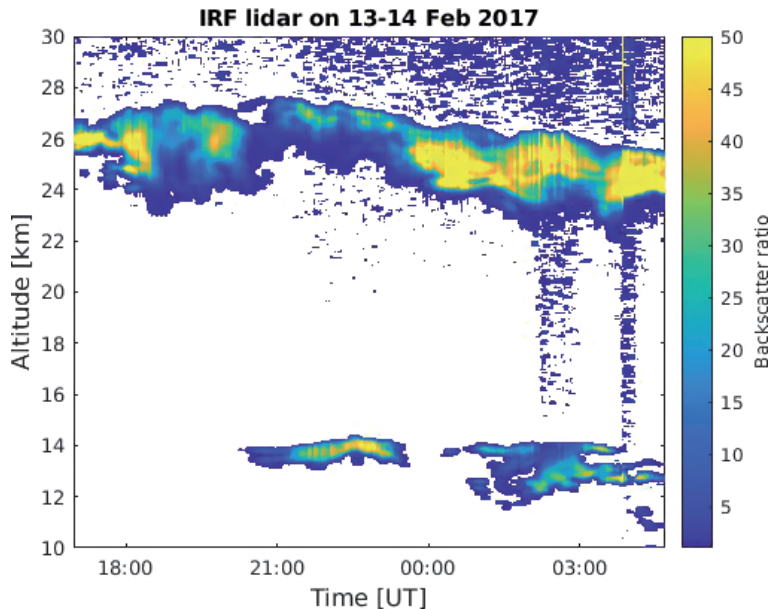

Fig. 3.   Backscatter ratio (BSR) from lidar observations of the PSC layer as the function of time and intensity on 13–14 February 2017. The backscatter signal in the parallel polarization channel is illustrated.
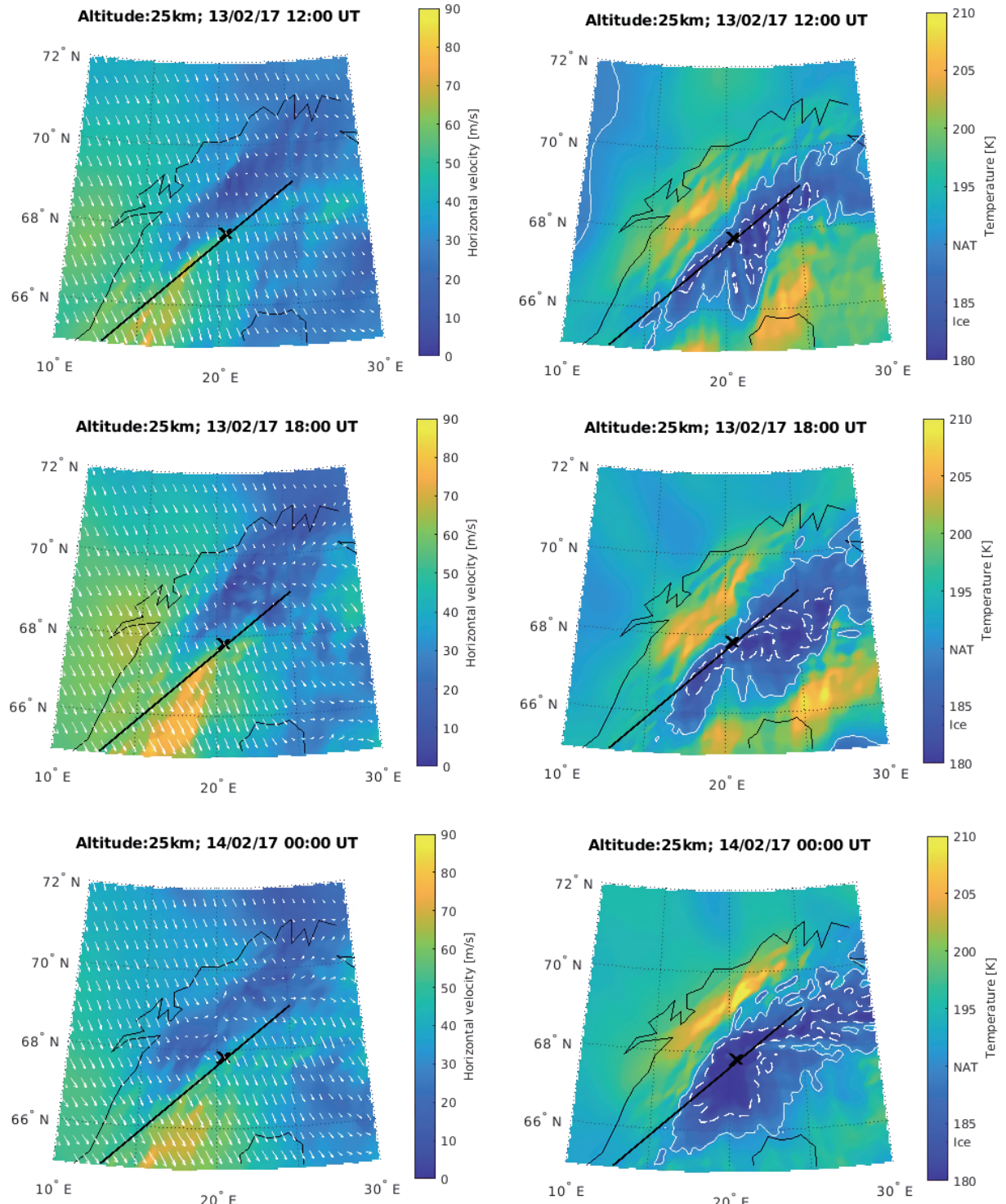
Fig. 4.   Horizontal maps of the wind velocity with wind vectors (left side) and temperature (right side) fields at a 25 km altitude for 12 UT, 18 UT on February 13th and 00 UT on February 14th as calculated by WRF. The black line (same as blue line in Fig. 2) marks the edge of the observed PSC. White lines indicate the existence temperatures for NAT particles (solid, Hanson and Mauersberger 1988) and ice particles (dashed, Marti and Mauersberger 1993).

13/02/17 and at 00 UT on date 14/02/17, as derived
with WRF. During all three times, wind directions
north of 65°N were roughly perpendicular to the Scan-
dinavian mountain range. Wind speed and direction
changed only marginally during this period. The wind
field induced a wave-like horizontal quasistationary
motion that resulted in a perturbation of the tempera-
ture field above and in the lee of the mountains. The
position and orientation of the main temperature min-
imum just behind the mountains corresponds well to
the position of the PSC edge at 12 UT and 18 UT on
February 13th, 2017. The orientation of the tempera-
ture minimum at 00 UT on February 14th corresponds
less to the orientation of the PSC edge. Visual obser-
vation of the development of the cloud edge was not
possible at that time of the day because of darkness.
However, our lidar observations proved the continuing
presence of a PSC layer. Additionally, the spaceborne
lidar CALIOP detected a PSC at approximately 69°N,
29°E while passing the Gulf of Bothnia east of Kiruna
during that night, shortly after 01 UT.

A commonly used indicator for the vertical stratifi-
cation of the atmosphere is the buoyancy frequency,
N, also called the Brunt–Väisälä frequency (see, e.g.,
Holton 1992). Figure 5 illustrates a cross section of N
through the location of the ground-based observations
and along the wind direction at 18 UT. One can see
that the first positive maximum is observed right
above the mountains at approximately 2 km; then,
other maxima occur at 14, 27–28, and 37–39 km
altitudes; hence, a vertical wavelength of the main
mountain wave is approximately 10–12 km above the
Kiruna area. The upward direction of energy propaga-
tion can be seen from the vertical phase propagation
directed downward relative to the mean flow (which
is from the left to right in Fig. 5) and westward rela-
tive to the mountains (Holton 1992). Two buoyancy
minima at 5 km and 10 km and two maxima at 14 km
and 28 km are directed westward relative to the moun-
tain ridge and with height. These phase tilts provide
the evidence of the upward wave energy propagation
as expected since the energy source for these waves
was located at the ground (mountains).

Figure 6 illustrates the temporal development of the
buoyancy frequency near the mountain crest at 69°N,
19°E (left panel) and in the lee of the mountains at
67.84°N, 20.41°E (right panel). Here, WRF was used
to achieve better time resolution than that achieved
with ERA5. At both locations, vertical profiles of
N remained fairly unchanged for approximately 24
hours, with wave-like structures. In Fig. 7, a profile
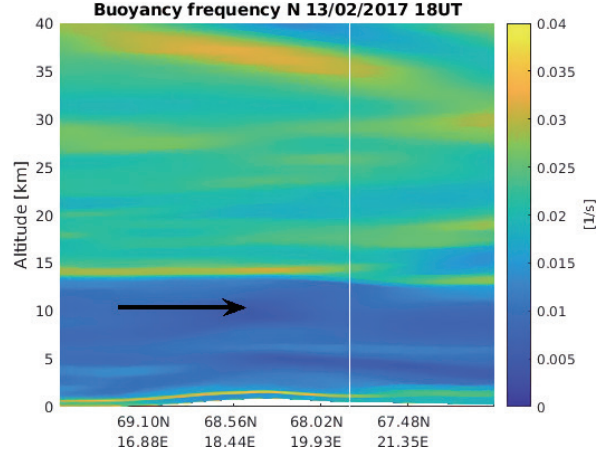for the buoyancy frequency near the mountain crest is

Fig. 5.   Buoyancy frequency variation calculated
from ERA5 data as a function of the geographical
position through the observational point along the
horizontal wind direction and altitude at 18 UT
on February 13th 2017. The horizontal axis gives
the geographical coordinates along the cross
section parallel to the horizontal wind direction.
The vertical white line depicts the position of the
lidar observational point. The height profile of
the Scandinavian mountain range along the cross
section is illustrated in white at the bottom of the
figure. The arrow indicates the direction of the
horizontal wind.

displayed. Although some temporal variation of ab-
solute numbers does occur, the height of the features
varies only marginally. Estimating the vertical length
of the wave-like motion is straightforward. It was
in the range of 10–12 km, both above the mountain
range and in the lee of the mountains where both
photos were taken and lidar measurements were per-
formed.

An apparently stationary wave in the lee of a moun-
tain is a special case of a topographic wave (see, e.g.,
Holton 1992). For a wave to appear to be stationary,
its phase speed c has to be exactly the opposite of the
speed of the mean flow $\bar{u}$. The dispersion relation for a
stationary wave is then

$$0 = \bar{u} \pm \frac{N}{\sqrt{k^2 + m^2}} \qquad (1)$$

Here, N is the buoyancy frequency, and k and m are
horizontal and vertical wavenumbers, respectively.
Note that Fig. 4 demonstrates the background wind
that is quasi-perpendicular to the PSC edge and is,
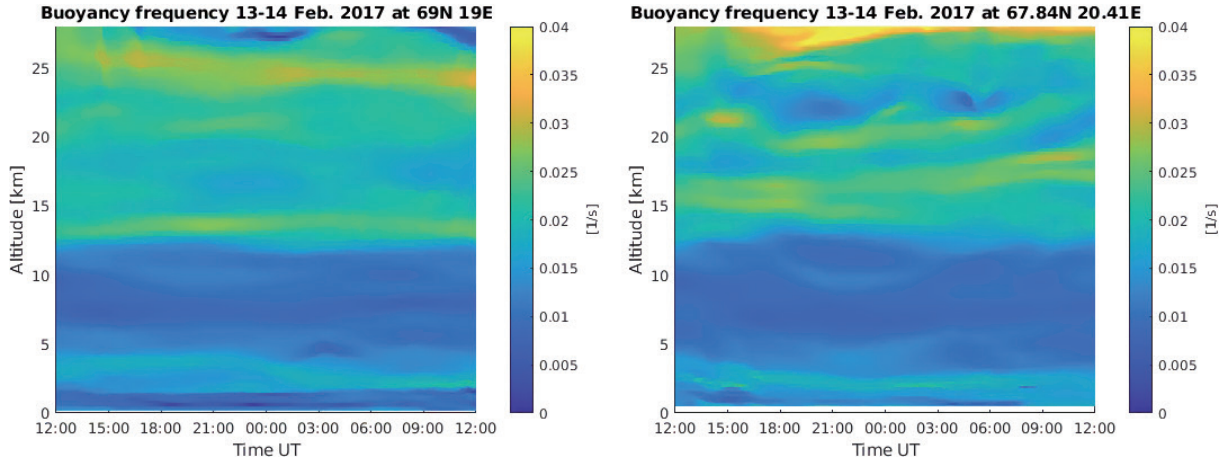hence, almost parallel to the k vector. Equation 1 can

Fig. 6.   Buoyancy frequency as a function of time as calculated with WRF. Left: near the mountain crest, right: at the location of lidar observations.
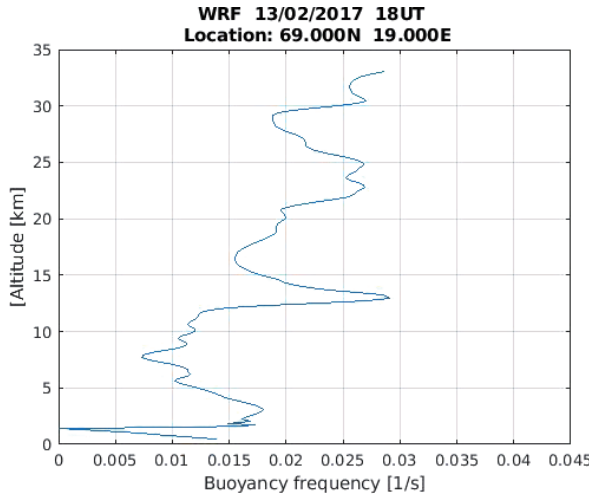

Fig. 7.   Profile of buoyancy frequency derived as calculated with WRF for a location near the mountain crest.
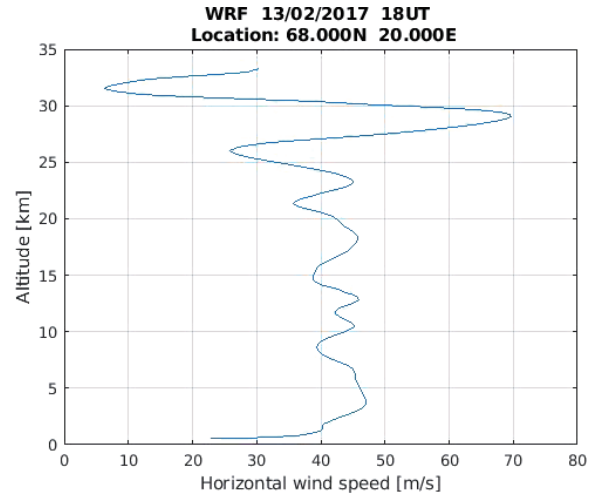
Fig. 8.   Profile of the horizontal wind speed perpendicular to the mountain crest (background horizontal wind along the horizontal wavenumber vector) as calculated with WRF. The location of the profile is near the mountain crest.

be simplified to

$$m^2 = \frac{N^2}{\bar{u}^2} - k^2 \qquad (2)$$

In our case, the horizontal wavelength is longer than 200 km, as one can see in Fig. 4; hence, $k < N/\bar{u}$. For a wave with a vertical wavelength of 12 km to be created, the horizontal wind speed should to be ~ 40 m s^{-1}. This means that the stationary wave was created at an altitude range where horizontal wind speed is around that value, i.e. in the lower troposphere

right above the mountains as demonstrated in Fig. 8. Figure 8 illustrates that the horizontal wind speed was varying around 40 m s^{-1} in the range of 35−45 m s^{-1} between 2 and 15 km. Small amplitude modulations of the mean wind speed between 5 km and 15 km are also seen because of interference of the stationary gravity wave with small-scale gravity waves. These small-scale modulations are also reproduced in the buoyancy frequency between 6 and 13 km seen in

Fig. 7. Since the vertical wavenumber m is a function of both the buoyancy frequency and mean wind speed (see Eq. 2), m might slightly change because of these small variations. However, the main period of the vertical wavelength of $10-12$ km is unchanged and is clearly seen in the buoyancy frequency (Fig. 7) and in the horizontal wind speed (Fig. 8) between 3 km and 13 km. Note that the horizontal wind speed, along the horizontal wavenumber vector, does not approach zero, meaning that there were no critical levels for mountain gravity waves propagating from the ground to the PSC altitude. The created mountain wave induced its own variations on the horizontal wind speed, resulting in high variations in the horizontal wind speed at higher altitudes above 15 km, with maximum wind speed changes of ~ 40 m s^{-1} at the 30 km altitude. Thus, theoretical considerations fit WRF model wind data that confirm a principal possibility of the formation of a stationary gravity wave above and in the lee of the mountains.

5. Summary

For the first time, a very long quasistationary (~ 600 km) and nearly straight polar stratospheric cloud edge was observed in Kiruna, Northern Sweden on February 13th, 2017. Both lidar observations and simulations with WRF indicated that atmospheric conditions were fairly unchanged for several hours. At the same time, strong winds were present across the Scandinavian mountain range and triggered the formation of mountain lee waves in the Kiruna area. It was demonstrated that the stationary waves that could be observed were formed by horizontal winds with a 40 m s^{-1} wind speed. Such wind speeds were found in the lower troposphere at an altitude of approximately 3 km. Hence, the waves that created the stationary cloud edge in the stratosphere propagated upwards from the lower troposphere.

References

Alexander, S. P., A. R. Klekociuk, A. J. McDonald, and M. C. Pitts, 2013: Quantifying the role of orographic gravity waves on polar stratospheric cloud occurrence in the Antarctic and the Arctic. *J. Geophys. Res.: Atmos.*, **118**, 11493–11507.

Blum, U., K. H. Fricke, G. Baumgarten, and A. Schöch, 2004: Simultaneous lidar observations of temperatures and waves in the polar middle atmosphere on the east and west side of the Scandinavian mountains: A case study on 19/20 January 2003. *Atmos. Chem. Phys.*, **4**, 809–816.

Blum, U., K. H. Fricke, K. P. Müller, J. Siebert, and G. Baumgarten, 2005: Long-term lidar observations of polar stratospheric clouds at Esrange in northern Sweden. *Tellus B*, **57**, 412–422.

Browell, E. V., C. F. Butler, S. Ismail, P. A. Robinette, A. F. Carter, N. S. Higdon, O. B. Toon, M. R. Schoeberl, and A. F. Tuck, 1990: Airborne lidar observations in the wintertime Arctic stratosphere: Polar stratospheric clouds. *Geophys. Res. Lett.*, **17**, 385–388.

Carslaw, K. S., M. Wirth, A. Tsias, B. P. Luo, A. Dörnbrack, M. Leutbecher, H. Volkert, W. Renger, J. T. Bacmeister, E. Reimer, and T. Peter, 1998: Increased stratospheric ozone depletion due to mountain-induced atmospheric waves. *Nature*, **391**, 675–678.

Dörnbrack, A., and M. Leutbecher, 2001: Relevance of mountain waves for the formation of polar stratospheric clouds over Scandinavia: A 20 year climatology. *J. Geophys. Res.*, **106D**, 1583–1593.

Dörnbrack, A., T. Birner, A. Fix, H. Flentje, A. Meister, H. Schmid, E. V. Browell, and M. J. Mahoney, 2002: Evidence for inertia gravity waves forming polar stratospheric clouds over Scandinavia. *J. Geophys. Res.*, **107D**, 8287, doi:10.1029/2001JD000452.

Fritts, D. C., and M. J. Alexander, 2003: Gravity waves dynamics and effects in the middle atmosphere. *Rev. Geophys.*, **41**, 1003, doi:10.1029/2001RG000106.

Hanson, D., and K. Mauersberger, 1988: Laboratory studies of the nitric acid trihydrate: Implications for the south polar stratosphere. *Geophys. Res. Lett.*, **15**, 855–858.

Hersbach, H., B. Bell, P. Berrisford, S. Hirahara, A. Horányi, J. Muñoz-Sabater, J. Nicolas, C. Peubey, R. Radu, D. Schepers, A. Simmons, C. Soci, S. Abdalla, X. Abellan, G. Balsamo, P. Bechtold, G. Biavati, J. Bidlot, M. Bonavita, G. De Chiara, P. Dahlgren, D. Dee, M. Diamantakis, R. Dragani, J. Flemming, R. Forbes, M. Fuentes, A. Geer, L. Haimberger, S. Healy, R. J. Hogan, E. Hólm, M. Janisková, S. Keeley, P. Laloyaux, P. Lopez, C. Lupu, G. Radnoti, P. de Rosnay, I. Rozum, F. Vamborg, S. Villaume, and J.-N. Thépaut, 2020: The ERA5 global reanalysis. *Quart. J. Roy. Meteor. Soc.*, **146**, 1999–2049.

Holton, J. R., 1992: *An Introduction to Dynamic Meteorology*. Academic Press, San Diego, 507 pp.

Kaifler, N., B. Kaifler, B. Ehard, S. Gisinger, A. Dörnbrack, M. Rapp, R. Kivi, A. Kozlovsky, M. Lester, and B. Liley, 2017: Observational indications of downward-propagating gravity waves in middle atmosphere lidar data. *J. Atmos. Sol.-Terr. Phys.*, **162**, 16–27.

Kirkwood, S., M. Mihalikova, T. N. Rao, and K. Satheesan, 2010: Turbulence associated with mountain waves over Northern Scandinavia–A case study using the ESRAD VHF radar and the WRF mesoscale model. *Atmos. Chem. Phys.*, **10**, 3583–3599.

Kohma, M., and K. Sato, 2011: The effects of atmospheric waves on the amounts of polar stratospheric clouds. *Atmos. Chem. Phys.*, **11**, 11535–11552.

Larsen, N., B. M. Knudsen, J. M. Rosen, N. T. Kjome, R. Neuber, and E. Kyrö, 1997: Temperature histories in liquid and solid polar stratospheric cloud formation. *J. Geophys. Res.*, **102D**, 23505–23517.

Marti, J., and K. Mauersberger, 1993: A survey and new measurements of ice vapor pressure at temperatures between 170 and 250K. *Geophys. Res. Lett.*, **20**, 363–366.

Maturilli, M., R. Neuber, P. Massoli, F. Cairo, A. Adriani, M. L. Moriconi, and G. Di Donfrancesco, 2005: Differences in Arctic and Antarctic PSC occurrence as observed by lidar in Ny-Ålesund (79°N, 12°E) and McMurdo (78°S, 167°E). *Atmos. Chem. Phys.*, **5**, 2081–2090.

Skamarock, W. C., J. B. Klemp, J. Dudhia, D. O. Gill, D. M. Barker, M. G. Duda, X.-Y. Huang, W. Wang, and J. G. Powers, 2008: *A description of the advanced research WRF, version 3*. NCAR Tech. Note, NCAR/TN-475+ STR, National Center for Atmospheric Research, Boulder, 113 pp.

Spang, R., L. Hoffmann, M. Höpfner, S. Griessbach, R. Müller, M. C. Pitts, A. M. W. Orr, and M. Riese, 2016: A multi-wavelength classification method for polar stratospheric cloud types using infrared limb spectra. *Atmos. Meas. Tech.*, **9**, 3619–3639.

Tabazadeh, A., R. P. Turco, K. Drdla, M. Z. Jacobson, and O. B. Toon, 1994: A study of type I polar stratospheric cloud formation. *Geophys. Res. Lett.*, **21**, 1619–1622.

Tilmes, S., R. Müller, A. Engel, M. Rex, and J. M. Russell III, 2006: Chemical ozone loss in the Arctic and Antarctic stratosphere between 1992 and 2005. *Geophys. Res. Lett.*, **33**, L20812, doi:10.1029/2006GL026925.

Voelger, P., and G. Nikulin, 2005: The new lidar system at the Swedish Institute of Space Physics in Kiruna: Description and first measurements. *Proceedings of the Seventeenth ESA Symposium on European Rocket and Balloon Programmes and Related Research*, Vol. 590, 321–325.

Voigt, C., A. Tsias, A. Dörnbrack, S. Meilinger, B. Luo, J. Schreiner, N. Larsen, K. Mauersberger, and T. Peter, 2000: Non-equilibrium compositions of liquid polar stratospheric clouds in gravity waves. *Geophys. Res. Lett.*, **27**, 3873–3876.